

1-15-2023

Strength and damage characteristics of tailings filling body with different particle size distributions

Ai-bing JIN

School of Civil and Resources Engineering, University of Science and Technology Beijing, Beijing 100083, China

Jie WANG

School of Civil and Resources Engineering, University of Science and Technology Beijing, Beijing 100083, China

Shuai-jun CHEN

School of Civil and Resources Engineering, University of Science and Technology Beijing, Beijing 100083, China

Hai LI

School of Civil and Resources Engineering, University of Science and Technology Beijing, Beijing 100083, China

Follow this and additional works at: <https://rocksoilmech.researchcommons.org/journal>



Part of the [Geotechnical Engineering Commons](#)

Custom Citation

JIN Ai-bing, WANG Jie, CHEN Shuai-jun, LI Hai, . Strength and damage characteristics of tailings filling body with different particle size distributions[J]. Rock and Soil Mechanics, 2022, 43(11): 3083-3093.

This Article is brought to you for free and open access by Rock and Soil Mechanics. It has been accepted for inclusion in Rock and Soil Mechanics by an authorized editor of Rock and Soil Mechanics.

Strength and damage characteristics of tailings filling body with different particle size distributions

JIN Ai-bing^{1,2}, WANG Jie^{1,2}, CHEN Shuai-jun^{1,2}, LI Hai^{1,2}

1. Key Laboratory of Ministry of Education for Efficient Mining and Safety of Metal Mine, University of Science and Technology Beijing, Beijing 100083, China

2. School of Civil and Resources Engineering, University of Science and Technology Beijing, Beijing 100083, China

Abstract: To explore the influence of tailings particle size distribution on strength and damage characteristics of filling body, uniaxial compression, scanning electron microscopy, and digital image correlation (DIC) tests were carried out on the filling body composed of ultrafine tailings (median particle size $D_{50}=10.1\ \mu\text{m}$), fine tailings ($D_{50}=37.1\ \mu\text{m}$), and coarse tailings ($D_{50}=121.31\ \mu\text{m}$), and the strength and microstructure characteristics were analyzed. Based on the cusp mutation theory, the damage identification index of the filling body was established using wavelet packet technology, and the damage characteristics of the filling body were quantitatively analyzed. The results reveal that the strength and elastic modulus of the filling body first increase and then decrease with the increase of D_{50} , but the influence of tailings particle diameter on the strength and elastic modulus of the filling body is reduced with the increase of slurry concentration. Compared with the ultrafine and coarse tailings filling body, the coarse and fine particles of the fine tailings filling body are more closely combined, and its porosity is the lowest and microstructure compactness is the best. The energy change rate (ECR) mutation point is defined as the threshold of the backfill specimen damage mutation, which is used to distinguish the stable damage stage and the accelerated damage stage of the specimen, and the damage mutations of the ultrafine, fine, and coarse tailings filling body occur when their stresses reach 92.83%, 92.31%, and 72.93% of the corresponding peak stresses. With the increase of D_{50} , the failure mode of the filling body changes from shear failure to tensile failure, with the ECR increasing from 20.65% to 28.25%, and the damage degree is gradually aggravated. The research results lay the foundation for improving the particle gradation of mine tailings and enhancing the strength of filling body.

Keywords: particle size of tailings; digital image correlation (DIC); wavelet packet energy spectrum analysis; micro damage identification index; cusp mutation theory

1 Introduction

As the most commonly used filling aggregate in metal mines, tailings are usually mixed with cementing materials and water to produce filling body with certain bearing capacities according to given mixture ratios^[1–3]. With the advancement of flotation process, the tailings with ultrafine particle size are becoming the mainstream in filling stopes, and their particle sizes have a significant impact on mechanical properties of filling body^[4]. Therefore, it is of great significance to study the influence of tailings particle size distribution on the strength and damage process of filling body, which helps improve tailings particle size distributions in mines.

Uniaxial compressive strength and damage characteristics of filling bodies are crucial indicators in evaluating their stability, and an amount of relevant research has been conducted taking tailings particle size distribution into account^[5–6]. Fall et al.^[7] carried out mechanical tests on filling bodies with different tailings fineness (proportion of tailings particles with particle size less than $20\ \mu\text{m}$) and found that the tailings with medium fineness are more conducive to enhancing the strength of filling body. Qiu et al.^[8] prepared artificial silicon tailings with different fineness and studied the influence of tailings fineness on the uniaxial compressive strength and ultrasonic

wave velocity of filling body. Ke et al.^[9] noticed that a certain amount of fine particles help improve the bulk density of coarse particles, thereby increasing the strength of filling body. Yang et al.^[10] explored the influence of tailings particle size composition on the strength of filling body and concluded that a good particle size composition contributes to increasing the strength of filling body when the filling ratio and concentration are the same. Kesimal et al.^[11] found that the greatest strength of filling body could be obtained when the proportion of tailings particles with particle size less than $20\ \mu\text{m}$ is 25%–27%. However, Xu et al.^[12] believed that too many or too few fine aggregates are detrimental to enhancing the strength of filling body. Cheng et al.^[13] determined the tailings particle gradation based on Talbol theory and obtained the relationship between particle gradation and failure characteristics of tailings through uniaxial compression tests. Yin et al.^[14] clarified the influence of coarse aggregate on the failure mode of filling body by implementing uniaxial compression tests on the filling body with mixed aggregates. Wu et al.^[15] believed that more coarse aggregates would aggravate early local stress concentration effects and block spalling in filling bodies. Zhou et al.^[16] proposed that the increase of coarse aggregate volume ratio would lead to the increase of crack extension range and tension crack proportion in concrete. Wu et al.^[17] found that too

Received: 28 December 2021

Revised: 16 July 2022

This work was supported by the National Natural Science Foundation of China (51804018, 52174106).

First author: JIN Ai-bing, male, born in 1974, PhD, Professor, mainly engaged in the teaching and research of rock mechanics and engineering. E-mail: jinaibing@ustb.edu.cn

coarse aggregate would result in more early failure zones and cracks in filling bodies during the loading process, and recommended the Talbot gradation index of aggregate adopted in mines should not be beyond 0.6. The above research just analyzes the strength characteristics of filling body and the failure mode of filling body from the perspective of cracks, but pays little attention to the microstructure and damage characteristics of filling body.

It has been proved that the digital image correlation (DIC) combined with the wavelet packet technology can be used to quantitatively characterize the crack damage process of concrete specimens^[18–19]. Lei et al.^[20] employed the DIC technology to observe the static three-point bending damage strain field of concrete specimens, decomposed DIC images through the wavelet packet technology, and obtained the early warning indicators of concrete crack initiation, which validated that the microcrack initiation location and damage degree could be accurately detected by the combined method. Zhou et al.^[21] adopted the three-dimensional DIC technology to conduct the observation and calculation of the four-point bending test on concrete beams, used the two-dimensional wavelet packet technology to analyze the principal strain contour, and defined the energy change rate (ECR) and the energy change rate standard deviation (ECRSD) as the micro damage identification indexes, thereby realizing the real-time positioning and observation of the micro damage on the specimen surface. Regarding the mutation phenomenon in the damage process of filling body, the cusp mutation theory can play a great role. Xu et al.^[22] characterized the region formed by the mutation of dissipative energy and elastic strain energy as the instability warning region of filling body based on the cusp mutation theory, which provides a new course for the early instability warning of filling body. Wang et al.^[23] established a cusp mutation model about the acoustic emission ring count to predict the instability of layered filling body. Therefore, the signal features in the DIC principal strain contour can be extracted and decomposed as the damage identification index of the specimen by the wavelet packet technology, and the damage mutation threshold can be determined based on the cusp mutation theory to accurately analyze the damage process of filling body.

In view of the above problems, this paper studies the strength characteristics and damage characteristics of tailings filling bodies with different particle size distributions. The tailings with different particle size distributions from Jinding Mine were chose to prepare the filling bodies. Uniaxial compression and scanning electron microscope (SEM) tests were carried out to analyze the influence of tailings particle size distribution on the strength characteristics and microscopic characteristics of filling body, and the principal strain contour of the damaged specimen was obtained through the DIC technology. Based on the wavelet packet technology and cusp mutation theory, the damage identification index of filling body specimen was

established, the ECR values of the specimen under different loading conditions were calculated, and the influences of tailings particle size distribution on the damage mutation process and failure mode of filling body were illustrated, which provides a method to quantitatively characterize the damage state of filling body with the aid of DIC. The research results can lay a foundation for improving the tailings particle size distribution and enhancing the strength of filling body.

2 Experimental design and method

After drying and particle size reduction of three kinds of tailings from Jinding Mine, the tailings, cement, and water were mixed to prepare the filling slurry according to the set slurry concentration and cement-sand ratio, and were then cured into a mold. After the curing age of specimens were reached, the uniaxial compression, DIC, and SEM tests on the specimens were carried out. In order to make the analysis results more consistent with the actual working conditions in the mine, different tailings used in the tests were all from Shandong Jinding Mining Co., Ltd., and the specific experimental workflow is shown in Fig. 1.

2.1 Test materials

After drying and reducing the particle size of three types of tailings, their particle size compositions were tested by LS-POP(9) laser particle size analyzer, and the particle size distribution curves of tailings were obtained, as shown in Fig. 2.

According to the measurement, the median particle sizes of the three types of tailings are 10.10 μm , 37.10 μm , and 121.31 μm , which corresponds to the ultrafine, fine, and coarse tailings, respectively. The cementing agent used in the test is P.O #42.5 cement, and the water is ordinary tap water.

In order to ensure that the chemical composition of the specimens have no influence on the test results, X-ray fluorescence spectroscopy (XFS) was carried out for the three types of tailings and cement, and the test results are shown in Table 1. One can see from Table 1 that the main chemical components of the three types of tailings are MgO, SiO₂, Fe₂O₃, and Al₂O₃, and the main chemical components of the cement are CaO, SiO₂, and Al₂O₃, all of which are conventional chemical components. The tailings do not contain special components (such as sulfide) that affect the strength of filling body^[24].

2.2 Specimen preparation and laboratory test

2.2.1 Specimen preparation

The tailings and cement were mixed according to the cement–sand ratio of 1:4 and the slurry concentration of 68%, 70%, and 72%, respectively. After being stirred uniformly, the mixtures were poured into molds with a size of 50 mm×50 mm×100 mm to prepare the filling body specimens. After 24 hours, the specimens were demoulded and placed in a constant temperature (20±1 °C) and humidity (95±1%) curing box for curing, and were taken out 60 days later for uniaxial compression tests.

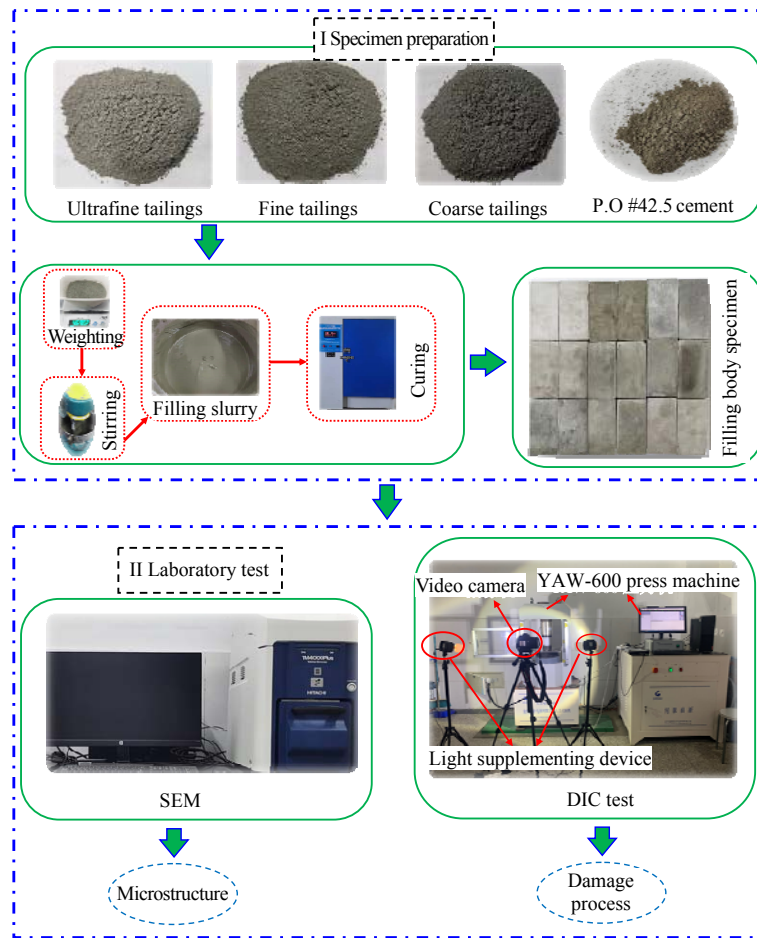


Fig. 1 Experimental workflow

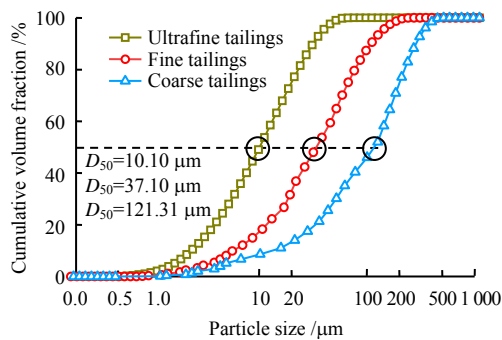


Fig. 2 Particle size distribution of tailings

Table 1 Chemical composition of tailings and cement

Compound	Mass fraction /%			
	Ultrafine tailings	Fine tailings	Coarse tailings	Cement
MgO	20.52	21.68	22.96	3.71
CaO	17.79	19.54	18.42	51.42
SiO ₂	38.02	36.89	39.49	24.99
Fe ₂ O ₃	10.87	9.87	10.57	4.03
Al ₂ O ₃	8.29	7.41	5.21	8.26
MnO	0.00	0.19	0.00	0.00
S	0.00	0.00	0.00	2.51
K ₂ O	1.86	0.69	0.37	3.31
Others	2.65	3.73	3.98	5.48

2.2.2 Uniaxial compression and DIC tests

YAW-600 rock mechanics testing machine was employed to conduct uniaxial compression on the

filling body specimens. The loading mode is displacement controlled. The specimen deformation is more uniform when the loading rate was 0.5–1.0 mm/min^[25]. Therefore, the loading rate was set as 0.5 mm/min. During the loading process, camera was used to capture the compression process, and the image acquisition frame rate was 60 frames/s. In order to make the damage process of specimen strictly correspond to the loading process on the specimen, the recording and loading were initiated at the same time. After the image acquisition was completed, the images were imported into the Vic-2D image analysis system for quantitative strain processing.

2.2.3 SEM test

After the strength tests, Hitachi TM4000Plus SEM was used to conduct SEM micro scanning on the filling body specimens to observe the influence of tailings particle size distribution on the microstructure of filling body specimen.

2.3 Wavelet packet damage index

Two-dimensional wavelet packet analysis can identify and decompose the characteristic signal of the image. Therefore, the DIC images are processed with the wavelet packet technology, and the damage signals of the specimens are extracted, decomposed, and reconstructed into energy feature vectors. Therefore, the structural damage can be indicated according to the energy change.

2.3.1 Wavelet packet decomposition principle

Wavelet packet transform is a linear Fourier transform that meets the law of energy conservation. At the same time, wavelet packet coefficients have energy dimensions and can be used for energy analysis^[26]. The wavelet packet is a linear combination of corresponding wavelet functions, which can be expressed as

$$\psi_{i,k}^j = 2^{i/2} \psi^j(2^i t - k) \tag{1}$$

where i , j , and k are integers, representing scale, modulation, and translation parameters, respectively; and T is the time parameter.

The selection of wavelet basis function directly determines the accuracy of wavelet packet calculation results. Therefore, it is necessary to select an appropriate type of wavelet function when image information is calculated and analyzed using wavelet packet transform. Daubechies wavelet, a commonly used wavelet transform, is mainly used for discrete wavelet transform, and it has the characteristics of orthogonality, biorthogonality, and tight support. Order N is a key parameter of Daubechies wavelet, and neither too large nor too small order N is conducive to the local focusing of signals in time domain. Therefore, an appropriate order N should be selected when Daubechies wavelet is selected for wavelet packet analysis. In general, the value of N is determined according to the norm energy entropy I^p (p is a constant, $1 \leq p \leq 2$)^[18], that is, it is determined by the following formula:

$$S_1(E_i) = \sum_{j=0}^{4^i-1} |E_{i,j}|^p \tag{2}$$

where $S_1(E_i)$ is the cost function of wavelet function; E_i is the total energy covering all frequency bands when the reconstructed signal is decomposed to the i th layer; and $E_{i,j}$ is the energy within the j th frequency band when the reconstructed signal is decomposed to the i th layer.

When wavelet packets are used to process image signals, the choice of decomposition levels has a significant impact on the accuracy of the calculation results. Three-layer wavelet decomposition is commonly used to obtain the energy spectrum characteristics of images^[21].

2.3.2 Signal feature vector extraction

After the DIC image is denoised and strengthened, the three-layer wavelet packet decomposition and node information reconstruction are performed. All the energy represented by each node is

$$E_{3,j} = \sqrt{\sum_{k=1}^n \sum_{l=1}^m x_{j,k,l}^2} \tag{3}$$

where $x_{j,k,l}$ ($j=0, 1, 2, \dots, 63$; $k=1, 2, \dots, n$; $l=1, 2, \dots, m$) refers to the amplitude of discrete points after signal reconstruction; and both n and m are the sizes of the image.

The energy within each frequency band (node)

after three-layer decomposition forms a new feature vector in frequency order. The new feature vector represents the energy information in the signal and forms the energy spectrum vector of the signal:

$$E_3 = [E_{3,0}, E_{3,1}, \dots, E_{3,63}] \tag{4}$$

2.3.3 Micro damage identification index determination

When the structural damage is identified by using wavelet packet, the increase of signal decomposition scale can reduce noise. Therefore, ECR within each frequency band of wavelet packet is taken as the damage identification index of specimen^[27–28]:

$$ECR = \sum_{j=0}^{63} \frac{|(E_{3,j})_d - (E_{3,j})_o|}{(E_{3,j})_o} \tag{5}$$

where $(E_{3,j})_o$ and $(E_{3,j})_d$ are the energy in each frequency band of the image when the filling body specimen is in the initial and damaged states, respectively.

2.4 Damage index mutation model

The damage process of the filling body specimen goes from gradual change to sudden change. When the load on the specimen reaches a certain level, the damage degree will change significantly, which can be quantitatively characterized by the cusp mutation theory. The damage degrees at different loading stages can be expressed by the ECR values of the images, which can be used as the criterion of mutation theory to provide a method to determine the damage mutation threshold of filling body.

As the loading process is displacement controlled, the ECR value of the specimen damage image is taken as the research object. A fourth order function expressing the relationship between ECR and ε is fitted with seven consecutive groups of data including ECR and ε values, and the fitting result is taken as the cusp mutation model at the center point^[29]:

$$ECR(\varepsilon) = \sum_{i=0}^4 \frac{\partial^i f}{\partial k^i} = \sum_{i=0}^4 a_i \varepsilon^i \tag{6}$$

where $ECR(\varepsilon)$ is the fitting function of the energy change rate; ε is the specimen strain; and a_i is the coefficient to be determined.

Using the Tschirnhaus transform, the cubic terms are eliminated, and $\varepsilon = x - a_3 / (4a_4)$ is introduced. When the strain is 0 and the fitting data contains $ECR(0)$, the ECR value of the specimen is 0, that is, $a_0 = 0$. However, when the fitting data do not include $ECR(0)$, a_0 is not 0, so Eq.(6) can be converted into a standard potential function^[30]:

$$ECR(x) = x^4 + ux^2 + vx + c \tag{7}$$

where u and v are mutation parameters; and c is a constant.

The parameters u and v are calculated by the following formula:

$$u = \frac{a_2}{a_4} - \frac{3a_3^2}{8a_4^2}, \quad v = \frac{a_1}{a_4} - \frac{a_2 a_3}{2a_4^2} + \frac{a_3^3}{a_4^3} \tag{8}$$

By finding the first and second derivatives of Eq.(7) and setting them to 0, the bifurcation set equation when ECR is used as a criterion can be obtained as

$$\Delta = 8u^3 + 27v^2 \tag{9}$$

where Δ is the mutation characteristic value, which is used to judge whether the mutation of ECR value at a certain point exists.

Therefore, the method to determine the damage threshold of filling body using ECR as the mutation criterion is described as follows:

(a) $\Delta > 0$, the specimen is not damaged or the damage is small;

(b) $\Delta < 0$, the damage of the specimen is relatively large, and the damage of the specimen at this moment is the damage mutation threshold of the filling body.

3 Strength characteristics analysis

3.1 Stress–strain curve

In view of the consistent influence of tailings particle size distribution on the stress–strain curve of filling body under different concentrations, the stress–strain curves of filling bodies with three types of tailings particle size distributions were analyzed, taking the case with the slurry concentration of 70% as an example. At the same time, the elastic moduli of filling bodies at different concentrations were analyzed, and the results are shown in Figs. 3 and 4.

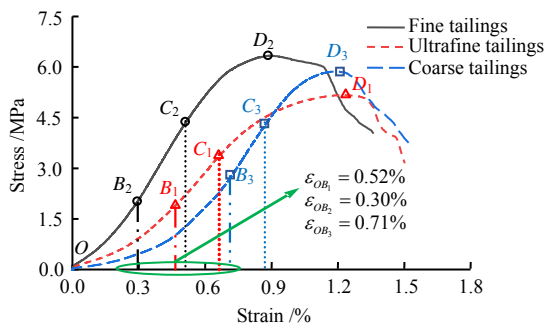


Fig. 3 Stress–strain curves of tailings filling bodies with slurry concentration of 70%

It can be observed from Fig. 3 that the pre-peak curves of tailings filling bodies with three particle size distributions can be roughly divided into three stages: micropore compaction stage (OB), elastic stage (BC), and plastic yield stage (CD). Comparative analysis manifests that the compaction stages of ultrafine, fine, and coarse tailings filling bodies end when the strains are 0.52%, 0.30%, and 0.71%, respectively, that is, the coarse tailings filling body has a longer compaction stage (OB_3), followed by the ultrafine tailings filling body (OB_1), and the fine tailings filling body has the shortest compaction stage (OB_2).

One can see from Fig. 4 that with the increase of slurry concentration, the elastic moduli of tailings

filling bodies with three particle size distributions gradually increase, but their differences decrease. When the slurry concentration is 68%, the elastic modulus of fine tailings filling body is 0.57 GPa, which is 24.5% and 19.29% higher than those of ultrafine and coarse tailings filling bodies, respectively. When the slurry concentration is 70%, the elastic modulus of fine tailings filling body is 0.86 GPa, which is 12.79% and 5.81% higher than those of ultrafine and coarse tailings filling bodies, respectively. When the slurry concentration is 72%, the fine tailings filling body has an elastic modulus of 0.96 GPa, which is 5.21% and 2.08% higher than those of ultrafine and coarse tailings filling bodies, respectively. The increase of slurry concentration reduces the influence of the tailings particle size distribution on the elastic modulus of filling body.

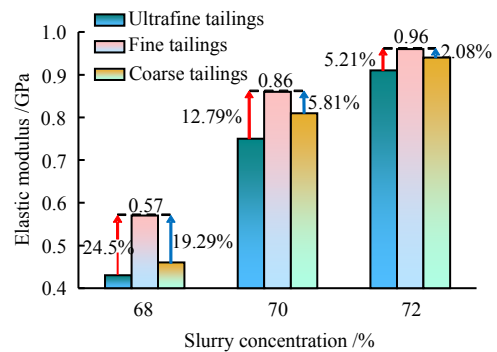


Fig. 4 Elastic moduli of tailings filling bodies with different particle size distributions

3.2 Uniaxial compressive strength

When the slurry concentrations are 68%, 70%, and 72%, the uniaxial compressive strengths of tailings filling bodies with three particle size distributions are shown in Fig. 5. The results show that with the increase of slurry concentration, the uniaxial compressive strengths of the ultrafine, fine, and coarse tailings filling bodies increase gradually, but their strength differences decrease gradually. When the slurry concentration increases from 68% to 72%, the uniaxial compressive strength of fine tailings filling body increases from 4.20 MPa to 6.85 MPa, while the uniaxial compressive strengths of ultrafine and coarse tailings filling body increase from 3.22 MPa and 3.42 MPa to 6.00 MPa and 6.30 MPa, respectively. The strength differences between the fine and ultrafine tailings filling bodies are reduced from 23.33% to 11.76%, and those between the fine and coarse tailings filling bodies are reduced from 18.57% to 7.35%, indicating that the increase of slurry concentration reduces the influence of the particle size distribution of tailings on the strength of filling body. Therefore, improving the slurry concentration may avoid the disadvantages of too fine or too coarse tailings when filling the mines.

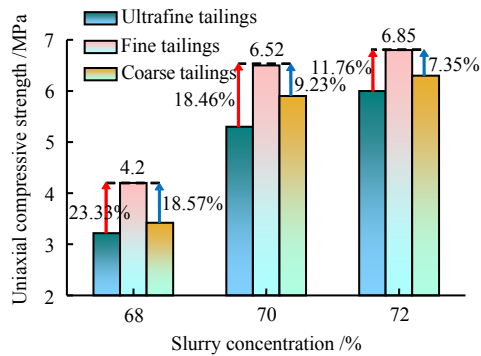


Fig. 5 Strengths of tailings filling bodies with different particle size distributions

3.3 Microstructure analysis

The microstructure of filling body includes the skeleton structure formed by the intersection of tailings aggregate and hydration products, and the pore structure composed of micropores and microcracks^[31]. SEM tests were conducted on the tailings filling body specimens with three particle size distributions, and the results are shown in Fig. 6. It can be seen from the figure that the ultrafine tailings filling body contains a lot of pore structures composed of micropores and microcracks, and there is an obvious weak boundary between pore structures and cement particles. The main pore structure in the coarse tailings filling body is the large gap between coarse particles, which tends to lead to local damage and microcrack growth when

compressed. There are few microcracks and weak structural planes in the fine tailings filling body, but hydration products (C-S-H gel and acicular ettringite) are more distributed and tightly wrap the large tailings particles, forming a relatively stable microstructure. In order to further characterize the differences in the microstructures of the filling bodies and explain the formation causes, Fig. 7 shows the schematic diagram of the microstructures of the tailings filling bodies with three particle size distributions. For the ultrafine tailings filling body, the particle sizes of most tailings are smaller than the cement fineness, and weak structural planes are easily produced. At the beginning of hydration, a large number of ultrafine particles are wrapped by water film and occupy the space of coarse particles, leading to a decrease in the filling density^[17]. With the extension of curing time, the water film gradually fades, and a large number of micropores are produced and connected to form microcracks, affecting the stability of the microstructure. For the coarse tailings filling body, although the tailings with large sizes can provide growth space for hydration products such as Aft, C-S-H gel, and Ca(OH)₂, the particle gap cannot be fully filled by hydration products when the content of cementing agent is small and the ratio of tailings with large sizes is large, resulting in more pore distribution and lower strength. The coarse and fine particles in the fine tailings filling body are closely arranged, and the particle gap is fully filled by hydration products, forming a stable skeleton structure.

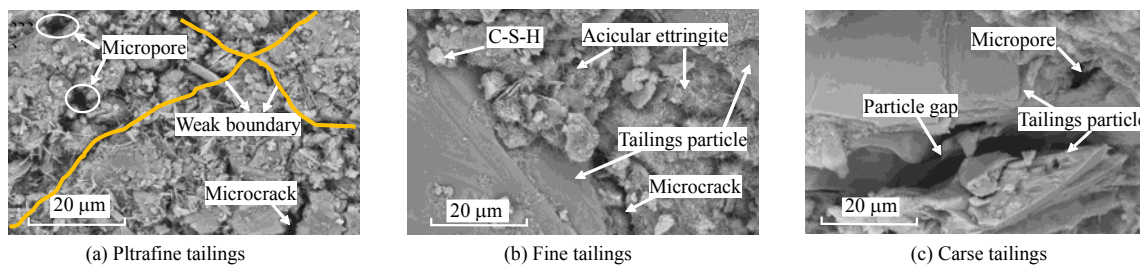


Fig. 6 Microstructure images of tailings filling bodies with different particle size distributions

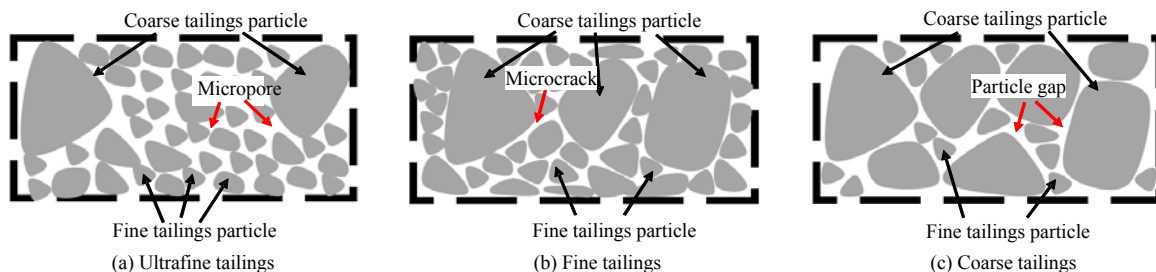


Fig. 7 Microstructure sketches of tailings filling bodies with different particle size distributions

In order to quantitatively characterize the difference of filling body microstructure, the SEM image is binarized and the porosity^[32] is calculated. The results are shown in Table 2. It can be seen from the table that the micro porosities of the ultrafine, fine, and coarse tailings filling bodies are 0.248, 0.183, and 0.200, respectively. The fine tailings filling body has the lowest porosity, fewer pore structures, and the densest

microstructure.

Based on the above analysis, the strength and microstructure characteristics of tailings filling bodies with different particle size distributions are obviously different. With the increase of D_{50} , the uniaxial compressive strength and elastic modulus of the filling body increase first and then decrease. The microscopic interpretation of this phenomenon is that the micro

porosity of the fine tailings filling body is smaller than that of the ultrafine and coarse tailings filling bodies, and the coarse and fine tailings particles are closely combined with the hydration products, forming a stable skeleton structure.

Table 2 Microscopic porosities of tailings filling bodies

Tailings	Number of black pixels /10 ⁷	Number of white pixels /10 ⁷	Number of whole pixels /10 ⁷	Porosity
Ultrafine	1.221	3.694	4.921	0.248
Fine	0.902	4.014	4.915	0.183
Coarse	0.987	3.931	4.918	0.200

4 Damage characteristics analysis

The damage characteristic of filling body is a key index to evaluate its mechanical properties. In this section, the DIC technology, wavelet packet technology, and cusp mutation theory were combined to conduct quantitative analysis on the damage characteristics of filling body, providing a basis for predicting the instabilities of tailings filling bodies with different particle size distributions.

4.1 Strain contour acquisition

The DIC technology can directly reflect the strain of specimen in the loading process through the color difference in the contour. The larger strain value means the more serious the damage. Figure 8 shows the distributions of DIC principal strain of fine tailings filling body under four axial strains when the slurry concentration is 70%. In the figure, ϵ_1 is the first principal strain.

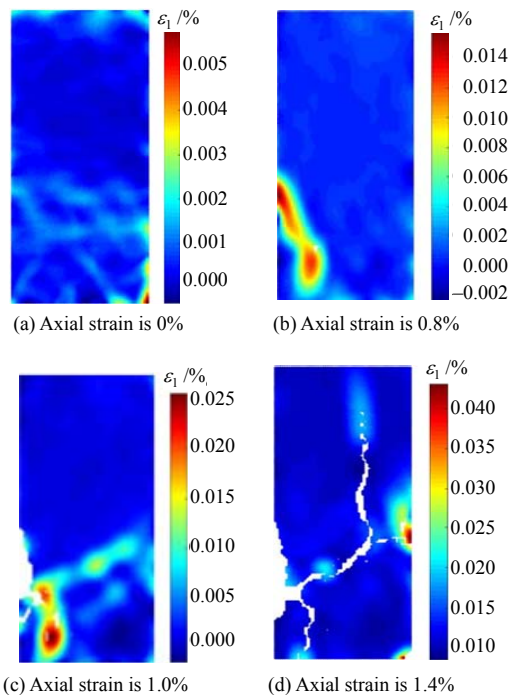


Fig. 8 Principal strain nephograms of damaged filling body specimen

Figure 8 illustrates that in the process of the axial strain of the specimen gradually developing from 0 to 1.4%, the strain concentration area first appears on the

right side of the specimen and continues to expand, and the damage degree continues to deepen, finally causing macro cracks. Therefore, after the DIC image is decomposed by wavelet packet, the energy signal within each frequency band will change with the change of the damage process, which can be used as the basis for identifying the surface damage of the specimen.

4.2 Wavelet function order determination

Two-dimensional wavelet packet analysis software is used to denoise the image. The image information in Fig. 8(a) is extracted, and the Daubechies wavelet is used for three-layer decomposition. An appropriate order N is determined according to Eq.(2) with p of 1.5, and the calculation results are shown in Table 3. It can be seen from the table that when the wavelet order is 10, the value of the cost function is the minimum. Therefore, db10 wavelet is selected to decompose the image.

Table 3 Cost functions of db wavelet with decomposition level of 3

Wavelet order N	$S_1(E_i) /10^{10}$	Wavelet order N	$S_1(E_i) /10^{10}$
7	1.919	14	1.981
8	1.982	15	1.938
9	1.917	16	1.957
10	1.916	17	1.996
11	1.975	18	1.957
12	1.924	19	1.986
13	1.931	20	2.006

4.3 Effect of particle size distribution on damage mutation

In the process of compression, the filling body successively experienced micropore compaction stage, elastic stage, plastic yield stage, and failure development stage. Among them, the plastic yield stage is considered as the key stage of crack initiation and development^[13]. The research shows that during the process of crack initiation, propagation, and extensive development, there is a damage mutation process in which the crack propagation speed increases rapidly^[14]. The process can be quantitatively characterized by a mutation point, which is defined as the damage mutation threshold. The DIC image is decomposed by wavelet packet to three layers, and the energy vector is reconstructed. The threshold value is determined by the mutation of the damage identification index. The relationship between the threshold value and the particle size distribution of tailings is summarized, which provides data support for determining the instabilities of tailings filling bodies with different particle size distributions.

When the slurry concentration is 70%, the relationships between the ECR–strain curve and the stress–strain curve of ultrafine, fine, and coarse tailings filling bodies are shown in Fig. 9. Meanwhile, in order to quantitatively express the mutation of ECR value, the characteristic ECR values at different strain stages are calculated by using the cusp mutation theory, and the calculation results are shown in Table 4.

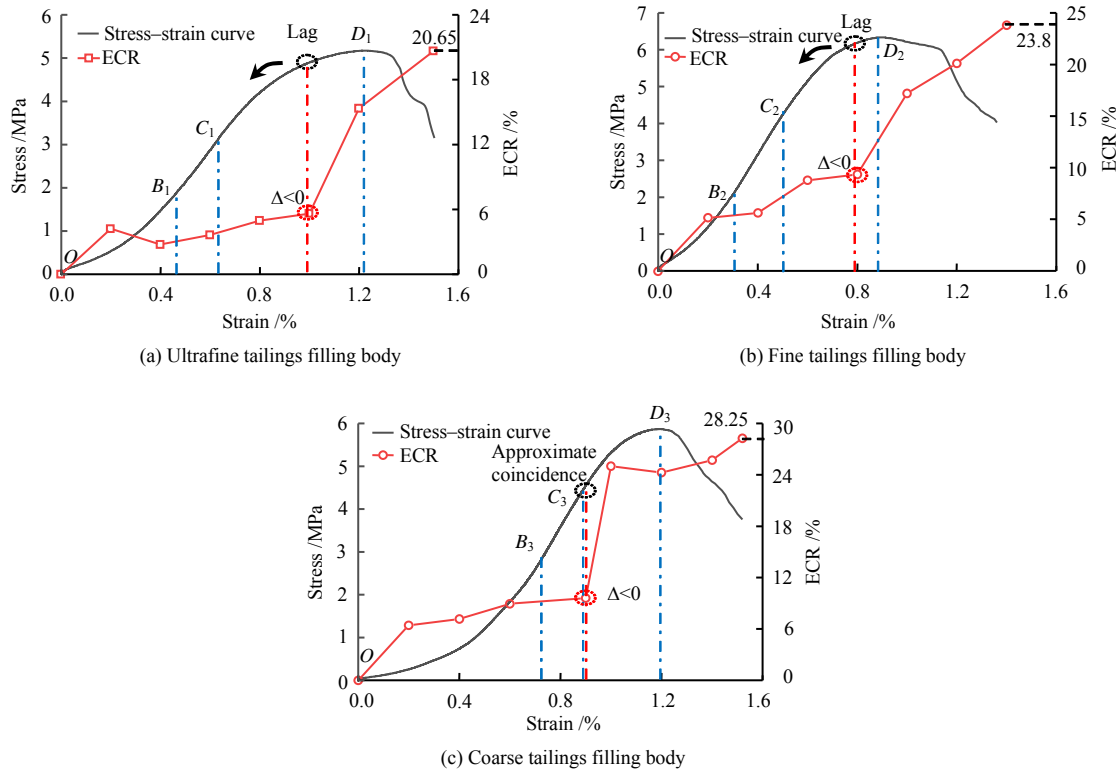


Fig. 9 Energy change rate curves with mutation segments of tailings filling bodies

Table 4 Characteristic mutation values of ECR index

Tailings	Strain /%	Fitting function	Characteristic value Δ	Mutation or not
Ultrafine tailings	0.8	$ECR(\varepsilon) = 611.6\varepsilon^4 - 1843\varepsilon^3 + 2041.9\varepsilon^2 - 978.4\varepsilon + 174.4$	4×10^{-4}	No
	0.9	$ECR(\varepsilon) = -140.4\varepsilon^4 + 643.8\varepsilon^3 - 987.7\varepsilon^2 + 633.5\varepsilon - 141.7$	0.195 5	No
	1.0	$ECR(\varepsilon) = -967.3\varepsilon^4 + 3822.7\varepsilon^3 - 5522\varepsilon^2 + 3472.1\varepsilon - 799.5$	-0.009 9	Yes
	1.1	$ECR(\varepsilon) = 144.84\varepsilon^4 - 801.25\varepsilon^3 + 1605.5\varepsilon^2 - 1354.8\varepsilon + 412.4$	0.084 8	No
Fine tailings	0.7	$ECR(\varepsilon) = -267.15\varepsilon^4 + 906.16\varepsilon^3 - 1064.6\varepsilon^2 + 530.26\varepsilon - 87.37$	0.009 1	No
	0.8	$ECR(\varepsilon) = -632.27\varepsilon^4 + 2033.7\varepsilon^3 - 2345.6\varepsilon^2 + 1163.7\varepsilon - 202.2$	-0.008 2	Yes
	0.9	$ECR(\varepsilon) = -661.31\varepsilon^4 + 2156.3\varepsilon^3 + 2526\varepsilon^2 + 1277.5\varepsilon - 228.25$	0.001 1	No
	1.0	$ECR(\varepsilon) = 947.7\varepsilon^4 - 3940.2\varepsilon^3 + 6026.2\varepsilon^2 - 3987.9\varepsilon + 971.85$	0.004 8	No
Coarse tailings	0.7	$ECR(\varepsilon) = 1768.5\varepsilon^4 - 4501.6\varepsilon^3 + 4186.1\varepsilon^2 - 1666.4\varepsilon + 247.83$	9.22×10^{-5}	No
	0.8	$ECR(\varepsilon) = -2424.7\varepsilon^4 + 7856.9\varepsilon^3 - 9112.1\varepsilon^2 + 4551.6\varepsilon - 829.9$	1.36×10^{-4}	No
	0.9	$ECR(\varepsilon) = -1668.9\varepsilon^4 + 5572.3\varepsilon^3 - 6745.9\varepsilon^2 + 3531.8\varepsilon - 668.76$	-0.009 3	Yes
	1.0	$ECR(\varepsilon) = 1988.5\varepsilon^4 - 8317.3\varepsilon^3 + 12808\varepsilon^2 - 8550.9\varepsilon + 2095.2$	9.16×10^{-4}	No

Figure 9 shows that ECR value increases with the gradual increase of filling body strain, indicating that the damage of the specimen is increased, and there are two stages of stable damage and accelerated damage in the process:

(a) In the stable damage stage, the ECR value of the filling body increases steadily and the value is small, which indicates that there is no obvious damage and stress concentration area in the specimen, and only the strain in the local area changes slightly, mainly in the micropore compaction stage and the early elastic stage.

(b) In the accelerated damage stage, the ECR value of the filling body increases rapidly and the value is large, which indicates that the strain concentration

area of the specimen gradually develops and the damage continues to increase.

The calculation results of the characteristic values in Table 4 show that the ECR values of ultrafine, fine, and coarse tailings filling bodies suddenly change when the strains are 1.0%, 0.8%, and 0.9%, respectively, that is, the damage mutation thresholds are 92.83%, 92.31%, and 72.93% of the peak stress, respectively. According to the stress–strain curves, there is a deviation between the mutation point and the starting point of plastic yield stage. The ECR value mutation points of ultrafine and fine tailings filling bodies lag behind the starting point of plastic yield stage, while the ECR value mutation point of coarse tailings filling body approximately coincides with the

starting point of plastic yield stage. The reason is that the ultrafine and fine tailings filling bodies are of high plasticity and poor brittleness, and it takes a long time for microcracks to develop extensively, leading to the damage mutation lagging behind the plastic yield stage. However, the coarse tailings filling body has poor plasticity and strong brittleness, and the stress concentration is easy to occur at the corners of coarse particles when compressed, which leads to the local damage mutation and plastic yield of the specimen almost synchronous.

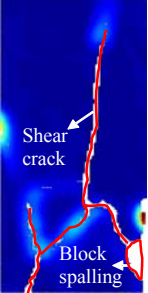

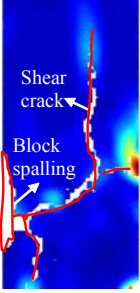
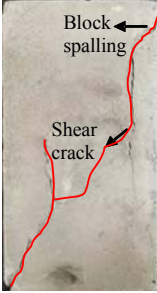
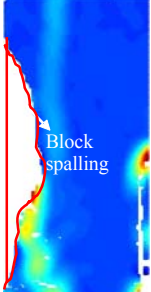
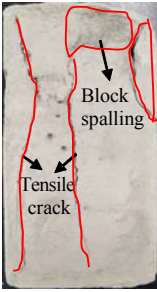
Based on the above analysis, the particle size distribution of tailings has a significant impact on the damage process of the filling body specimen. Excessive coarse tailings particles will cause premature damage mutation of the specimen and lead to instability of the filling body. Therefore, the strength and damage characteristics of filling body should be comprehensively considered when filling the goaf, and the tailings size

distribution should be reasonably selected.

4.4 Effect of particle size distribution on fracture mode

As seen from Fig. 9, the development trends of ECR values of tailings filling bodies with different particle size distributions are basically the same, but the degrees are different, especially at the failure stage. The ECR value of coarse tailings filling body is obviously large. Here, the case with the slurry concentration of 70% is given. According to the loading ending condition (60% of the peak stress), the ECR values of the post-peak failure nodes (corresponding to 59.43%, 61.81%, and 62.71% of the respective peak stress) of the tailings filling bodies with three particle size distributions are selected for comparison combined with the actual failure characteristics of the specimen, the impact of the tailings particle size distribution on the fracture mode of filling body is analyzed. The results are shown in Table 5.

Table 5 ECR indices and DIC nephograms of filling bodies at failure point

Tailings	DIC contour at failure	Failure pattern	ERC value at failure /%
Ultrafine tailings			20.65
Fine tailings			23.8
Coarse tailings			28.25

It can be seen from Table 5 that with the increase of D_{50} , the ECR value and damage degree of filling body at failure gradually increase. Combined with the DIC principal strain nephogram of the specimen and the actual failure pattern, the following conclusions can be drawn: for the ultrafine tailings filling body, the failure pattern is mainly semi-penetration shear failure,

the relative displacement on both sides of the crack is small, the damage degree is relatively small, and the ECR value is only 20.65%; for the fine tailings filling body, the failure pattern presents penetration shear failure accompanied by relatively large block spalling, the relative displacement on both sides of the crack is large, the damage degree is large, and the ECR value

increases to 23.8%; for the coarse tailings filling body, the failure pattern is dominated by penetration tensile failure accompanied by large-scale block spalling, the specimen is seriously damaged, and the ECR value reaches 28.25%.

Due to the non-uniformity of the tailings particle size distribution, the crack growth of the specimen shows no obvious regularity. Therefore, this section focuses on the damage characteristics of the tailings filling bodies with different particle size distributions according to the change of ECR value. It is found that with the increase of the D_{50} , the local damage mutation of the filling body gradually advances, the damage degree continues to increase, and the failure pattern gradually changes from shear failure to tension failure, accompanied by local spalling. The dynamic damage process can be quantitatively revealed by this method for the specimen specimen with obvious crack growth rules, and the failure mechanism of filling body can be further analyzed. Additionally, how to further optimize the tailings particle size used in mines according to the results of this study will be the focus of the next study.

5 Conclusions

(1) With the increase of D_{50} , the uniaxial compressive strength and elastic modulus of filling body increase first and then decrease. With the increase of slurry concentration, the influence of tailings particle size on the strength and elastic modulus of filling body decreases.

(2) From the microscopic point of view, the difference in tailings particle size distributions will cause the difference in filling body microstructures. The coarse and fine particles of the fine tailings filling body are closely combined and tightly wrapped by hydration products, which leads to the lowest porosity and form a stable skeleton structure, and the microstructure compactness of the fine tailings filling body is the best.

(3) According to the variation trend of ECR value of filling body, the damage process is divided into stable damage stage and accelerated damage stage. By calculating the mutation characteristic value of ECR value, it is found that the ECR values of the ultrafine, fine, and coarse tailings filling bodies change abruptly at 92.83%, 92.31%, and 72.93% of their peak stresses, respectively. The mutation point is not completely consistent with the starting point of the plastic yield stage. The larger the D_{50} is, the more forward the mutation point is, and the earlier the filling body failure occurs.

(4) According to DIC principal strain nephogram, failure pattern, and ECR value of filling body at failure, with the increase of D_{50} , the ECR value of filling body gradually increases from 20.65% to 28.25%, and the corresponding failure pattern converts from shear failure to tensile failure accompanied by large block spalling, indicating that the filling body failure will be more severe if the tailings particle size

is too large.

The research results show that it is feasible to judge the damage state and failure pattern of filling body through the ECR value, which effectively avoids the subjective and random shortcomings of the visual measurement of the specimen damage, and provides a new idea for the quantitative characterization of the filling body damage state.

References

- [1] WU Hao, ZHAO Guo-yan, CHEN Ying, et al. Deformation mechanism of un-cemented filling materials and grading in confined compaction tests[J]. *Journal of Mining & Safety Engineering*, 2018, 35(6): 1225–1232.
- [2] WEI Xiao-ming, GUO Li-jie, ZHOU Xiao-long, et al. Full sequence stress evolution law and prediction model of high stage cemented backfill[J]. *Rock and Soil Mechanics*, 2020, 41(11): 3613–3620.
- [3] JIN Ai-bing, JU You, SUN Hao, et al. Pore structure and strength deterioration mechanism of phase change energy storage backfill[J]. *Rock and Soil Mechanics*, 2021, 42(10): 2623–2633.
- [4] XIAO Bo-lin, MIAO Sheng-jun, GAO Qian, et al. Study on solidification characteristics of metallurgical slag binder materials for ultra-fine tailings backfill[J]. *The Chinese Journal of Nonferrous Metals*, 2022, 32(4): 1152–1163.
- [5] CHENG Hai-yong, WU Ai-xiang, WU Shun-chuan, et al. Research status and development trend of solid waste backfill in metal mines[J]. *Chinese Journal of Engineering*, 2022, 44(1): 11–25.
- [6] QIU J P, YANG L, SUN X G, et al. Strength characteristics and failure mechanism of cemented super-fine unclassified tailings backfill[J]. *Minerals*, 2017, 58(7): 1–13.
- [7] FALL M, BENZAAZOUA M, OUELLET S. Experimental characterization of the influence of tailings fineness and density on the quality of cemented paste backfill[J]. *Minerals Engineering*, 2004, 18(1): 41–44.
- [8] QIU J P, GUO Z B, YANG L, et al. Effect of tailings fineness on flow, strength, ultrasonic and microstructure characteristics of cemented paste backfill[J]. *Construction and Building Materials*, 2020, 263: 120645.
- [9] KE X, HOU H B, ZHOU M, et al. Effect of particle gradation on properties of fresh and hardened cemented paste backfill[J]. *Construction and Building Materials*, 2015, 96: 378–382.
- [10] YANG Liu-hua, WANG Hong-jiang, WU Ai-xiang, et al. Gradation optimization of unclassified tailings paste with Gobi aggregates[J]. *The Chinese Journal of Nonferrous Metals*, 2016, 26(7): 1552–1558.
- [11] KESIMAL A, ERCIKDI B, YILMAZ E. The effect of desliming by sedimentation on paste backfill performance[J]. *Minerals Engineering*, 2003, 16(10): 1009–1011.
- [12] XU Wen-bin, DU Jian-hua, SONG Wei-dong. Experiment

- on the mechanism of consolidating backfill body of extra-fine grain unclassified tailings and cementitious materials[J]. *Rock and Soil Mechanics*, 2013, 34(8): 2295–2302.
- [13] CHENG Ai-ping, DONG Fu-song, SHU Peng-fei, et al. Mechanical properties and acoustic emission characteristics of continuous graded cemented backfill[J]. *Journal of Huazhong University of Science and Technology (Natural Science Edition)*, 2021, 49(8): 46–52.
- [14] YIN Sheng-hua, HOU Yong-qiang, YANG Shi-xing, et al. Analysis of deformation failure and energy dissipation of mixed aggregate cemented backfill during uniaxial compression[J]. *Journal of Central South University (Science and Technology)*, 2021, 52(3): 936–947.
- [15] WU Jiang-yu, JING Hong-wen, PU Hai, et al. Macroscopic and mesoscopic mechanical properties of cemented waste rock backfill using fractal gangue[J]. *Chinese Journal of Rock Mechanics and Engineering*, 2021, 40(10): 2083–2100.
- [16] ZHOU X, XIE Y J, LONG G S, et al. Effect of surface characteristics of aggregates on the compressive damage of high-strength concrete based on 3D discrete element method[J]. *Construction and Building Materials*, 2021, 301: 101–124.
- [17] WU J Y, FENG M M, MAO J M, et al. Particle size distribution of aggregate effects on mechanical and structural properties of cemented rockfill: experiments and modeling[J]. *Construction and Building Materials*, 2018, 193: 295–311.
- [18] YANG K M, CUI Y H, QIAN X. A method on obtaining best wavelet packet decomposition level and reducing noise of hyperspectral image[J]. *Sensor Letters*, 2013(6): 1042–1049.
- [19] HE H X, ZHENG J C, LIAO L C, et al. Damage identification based on convolutional neural network and recurrence graph for beam bridge[J]. *Structural Health Monitoring*, 2021, 20(4): 1392–1408.
- [20] LEI D, YANG L Q, XU W X, et al. Experimental study on alarming of concrete micro-crack initiation based on wavelet packet analysis[J]. *Construction and Building Materials*, 2017, 149: 716–723.
- [21] ZHOU K Y, LEI D, HE J T, et al. Real-time localization of micro-damage in concrete beams using DIC technology and wavelet packet analysis[J]. *Cement and Concrete Composites*, 2021, 123: 104198.
- [22] XU Xiao-dong, SUN Guang-hua, YAO Xu-long, et al. A cusp catastrophe warning model for instability of backfill based on energy dissipation and release[J]. *Rock and Soil Mechanics*, 2020, 41(9): 3003–3012.
- [23] WANG J, FU J X, SONG W D, et al. Acoustic emission characteristics and damage evolution process of layered cemented tailings backfill under uniaxial compression[J]. *Construction and Building Materials*, 2021, 295: 123663.
- [24] WU J Y, FENG M M, NI X Y, et al. Aggregate gradation effects on dilatancy behavior and acoustic characteristic of cemented rockfill[J]. *Ultrasonics*, 2019, 92: 79–92.
- [25] XIU Z G, WANG S H, JI Y C, et al. Loading rate effect on the uniaxial compressive strength (UCS) behavior of cemented paste backfill (CPB)[J]. *Construction and Building Materials*, 2020, 242: 118–132.
- [26] ZHOU K Y, LEI D, HE J T, et al. Single micro-damage identification and evaluation in concrete using digital image correlation technology and wavelet analysis[J]. *Construction and Building Materials*, 2021, 267: 120951.
- [27] ZHAO B N, LEI D, FU J J, et al. Experimental study on micro-damage identification in reinforced concrete beam with wavelet packet and DIC method[J]. *Construction and Building Materials*, 2019, 210: 338–346.
- [28] GUO X, LI Y, SUO T, LIANG J. De-noising of digital image correlation based on stationary wavelet transform[J]. *Opt and Lasers in Engineering*, 2017, 90: 161–172.
- [29] QI Kuan. Study on performance of cemented backfill materials with unclassified tailings and stability of stope surrounding rock in Yongping copper mine[D]. Beijing: University of Science and Technology Beijing, 2018.
- [30] XUE Xiao-hui, LIU Tie-li, ZHOU Yi-tao. Safety evaluation and accident treatment of foundation pit based on cusp catastrophe theory and R/S analysis[J]. *Geotechnical Investigation & Surveying*, 2022, 50(7): 15–21.
- [31] WU J Y, FENG M M, HAN G S, et al. Experimental investigation on mechanical properties of cemented paste backfill under different gradations of aggregate particles and types and contents of cementing materials[J]. *Advances in Materials Science and Engineering*, 2019(1), 9456861.
- [32] XU Wen-bin, CAO Pei-wang, CHENG Shi-kang. Study on fracture characteristics and crack propagation mode of cemented backfill in deep mine[J]. *Journal of Central South University (Science and Technology)*, 2018, 49(10): 2508–2518.